An Application of Modal Decomposition to Supersonic Flow Over a Wall-Mounted Turret

Undergraduate Honors Thesis

A Thesis Presented in Partial Fulfillment of the Requirements for Graduation with Honors Distinction in the Department of Aerospace Engineering at The Ohio State University

By

Mikala Malkus

April, 2020

Under The Advisement of Dr. Datta Gaitonde

Abstract

Data driven modal decomposition techniques provide a means for extracting physically important features from high-dimensional, time-resolved dynamic systems. While the theoretical bases of these methods are well-developed, the interpretation of the obtained modes to understand complex unsteady flow physics can be difficult. In this research, the Proper Orthogonal Decomposition (POD) and Dynamic Mode Decomposition (DMD) techniques were employed to study the unsteady behavior of supersonic flow over a wall-mounted cylindrical turret. This flow problem contains a variety of time-dependent features including multiple unsteady shock waves and separated shear layers. The multiscale and broadband nature of these features lend themselves well to be examination via the above modal decomposition techniques which extract modes based on characteristics such as energy content and frequency. The POD method was used to objectively rank the dominant features in the system while the DMD method highlighted structures based on their dynamics and their evolution with time. The analysis indicates that unsteady shock waves dominate many aspects of the unsteadiness in this flow, since the top POD mode contained over 40% total energy. Lower ranked POD modes yielded detail about structures in the shear layer and separation regions; however, these were mixed and broadband in character. The DMD modes revealed that the unsteady shock waves were oscillating at a peak nondimensional frequency of $St_L \sim 0.3$, about an order of magnitude lower than the next extracted mode. Since DMD modes contain only a single frequency, other modes extracted coherent oscillation patterns in the shear layers, separation regions, and turbulent boundary layers. Overall, it was found that DMD provided a better characterization of all unsteady features in the flow. Although the application was complex, modal decomposition was shown to be a useful tool for characterization of the features dominating the unsteady flows, which is vital for flow control techniques to be developed. Future work should focus on the development of reduced order models for use in flow control analyses.

Acknowledgments

I would like to sincerely thank my advisor, Dr. Datta Gaitonde, for providing me with the opportunity to develop, conduct, and own my research as an undergraduate student. While some goals seemed distant at times, his encouragement always brought them within reach. With his continuous guidance over the past two years, I have gained technical confidence as engineer, but more importantly, grown tremendously as a person. I am thankful to have him as a mentor and to continue this journey in graduate school.

I was very fortunate to have the support and guidance of many of the graduate students in my lab throughout this project. First, I would like to thank Matthew Aultman for helping to integrate me into the lab and being very willing to answer even the simplest of questions. I also need to thank Rajesh Ranjan for being a great teacher in the world of modal decomposition. With your help, I was able to gain a deep knowledge of the theory and application these methods, in just two short semesters. Many others in my lab helped me along the way, answering all of my questions and ensuring that I was successful in all aspects of this project. I want to thank everyone for their guidance.

Finally, I would like to thank my family and friends for supporting and guiding me throughout all my endeavors in life. I would not be here without them and I am thankful for their support.

Contents

List of Figures **4**

1 Introduction **5**

1.1 Modal Decomposition 5

1.1.1 Proper Orthogonal Decomposition (POD) 9

1.1.2 Dynamic Mode Decomposition (DMD) 11

1.2 Supersonic Flow Over a Wall-Mounted Turret 14

1.2.1 Flow physics description 15

1.2.2 Application of Modal Decomposition 18

2 Methods **20**

2.1 Data Format Description 20

2.2 Proper Orthogonal Decomposition 21

2.3 Singular Value Decomposition 23

2.4 Dynamic Mode Decomposition 24

3 Results **28**

3.1 Database description 28

3.2 Convergence Validation 28

3.3 POD Results 30

3.4 DMD Results 35

4 Conclusion **40**

A POD Matlab Code **42**

B DMD Matlab Code **44**

List of Figures

1.1 Von Kármán vortices swirl in the clouds downwind of Isla Soco, a volcanic island off the coast of Mexico (Image Credit: NASA) 6

1.2 Modal decomposition of two-dimensional flow over a flat plate (Re = 100) [11] 8

1.3 Instantaneous snapshot of flowfield density 15

1.4 Streamlines describing unsteady features in supersonic flow past a wall-mounted cylinder from ref. [21] 16

1.5 Schematic of unsteady features in supersonic flow around a turret [24] 17

3.1 Density mean flow 29

3.2 Streamwise velocity mean flow 29

3.3 Density and streamwise velocity POD mode energies 30

3.4 Density and streamwise velocity fluctuations, sum of POD mode energies . . 31

3.5 Density field fluctuations, first POD mode associated with shock motion, energy $\sim 45\%$ 32

3.6 Streamwise velocity field fluctuations, first POD mode associated with shock motion, energy $\sim 11\%$ 32

3.7 Higher-order Density POD modes 33

3.8 DMD frequency spectrum 36

3.9 Density field low-frequency DMD Mode $St_L \sim 0.3$ 37

3.10 Streamwise Velocity field low-frequency DMD Mode $St_L \sim 0.3$ 38

3.11 Density field intermediate-frequency DMD Mode $St_L \sim 11.5$ 39

3.12 Density field high-frequency DMD Mode $St_L \sim 30$ 39

Chapter 1: Introduction

1.1 Modal Decomposition

The ability to study complex fluid flow phenomena is becoming increasingly viable due to recent advances in both computational and experimental methods. The increase in scale resolving and computing capabilities allow for flow features in realistic problems to be determined to extremely high spatio-temporal detail. As a result, a large number of high-fidelity datasets are readily available or can be generated quickly. However, it can be difficult to analyze such datasets because of their size. Although seemingly disorganized, many contain low-dimensional features that serve as a foundation to the underlying dynamics. The emergence and persistence of such features indicates that many high-dimensional problem may be represented in a simpler form for various purposes. Modal decomposition offers a means for extracting these low-dimensional dynamics directly from computational or experimental data. When organization is found, the underlying physics can be better understood, thus providing a means to identify mechanisms for flow control.

One of the goals of modal decomposition is to provide physical insight to the dynamic behavior of a system by extracting and organizing low-dimensional features, often called called model order reduction. In fluid dynamics, these features are often called coherent structures, because they persist in the flow and dominate the spatial and temporal dynamics, thus suggesting they are dynamically important. A common example is von Kármán shedding [1, 2], where patterns in the large-scale vortical structures and time-dynamics are easily distinguishable. Von Kármán shedding appears in many different forms of separated flows, including structures in the atmosphere seen from space as clouds moves past a large volcanic island as seen in figure 1.1.

Figure 1.1: Von Kármán vortices swirl in the clouds downwind of Isla Soco, a volcanic island off the coast of Mexico (Image Credit: NASA)

The observation of these organized features motivates their extraction by modal decomposition, even in complex turbulent flows where large structures may not be so obvious [3]. Once these dominant structures are identified, they provide a means for reducing the complexity of the problem by describing it in a low-dimensional, organized form.

Two commonly used modal decomposition methods are the Proper Orthogonal Decomposition (POD) and the Dynamic Mode Decomposition (DMD). Their widespread use is partly attributed to the fact that their algorithms are linear procedures and easily implemented, although the dynamical system they normally analyze are nonlinear. These are both mathematical techniques, which serve a similar purpose; decompose a time-resolved flowfield into spatial modes accompanied by characteristic values, including time variation, that reveal key features of the energy or the dynamics of each mode. The methods discussed are referred to as data-driven methods because they only take flowfield data as input, meaning they require

no prior knowledge of the governing equations in order to extract the dominant dynamics. Both POD and DMD are deeply rooted in eigenvalues or singular values and employ Singular Value Decomposition (SVD) to obtain the modes. These are used to break down the flowfield into its characteristic basis vectors and, by suitably neglecting smaller contributions, obtain a more compact representation of the high-dimensional dynamic systems.

Modal decomposition has become common practice in the analysis of fluid flows, with a surge of activity in recent decades. As the methods have developed, their ability to extract dominant features from both simulation and experiments in benchmark flows have been demonstrated [4, 5, 6]. The application of methods like POD and DMD have become so widespread that they are now discussed in textbooks [7, 8]. As computational technology has advanced and high-fidelity datasets have become increasingly available, the capability of these methods to extract coherent structures in high-fidelity simulations has been relatively well demonstrated. Some examples include analyzing vortex shedding in the flow behind a high-speed train [9] and investigating pressure perturbation sources on a launch vehicle afterbody [10].

An example of a modal decomposition applied to incompressible flow over a flat plate can be seen in figure 1.2. From the instantaneous snapshots, a von Kármán vortex street is observed in the wake behind the plate. When POD is applied to the fluctuating component of this flow, it is able to discern the major oscillation patterns of fluctuating velocity in the wake, as well as their quantitative contribution to the overall variance of the system. Because this flow is relatively low-dimensional to begin with (the Reynolds number is 100, which is relatively small), it only requires the first two oscillatory modes and the mean flow to almost fully reconstruct the time-varying flowfield. If the Reynolds number were increased and turbulence set in to create smaller structures in the wake, the energy content of the first two modes would decrease and the number of modes required to reconstruct the flow would increase.

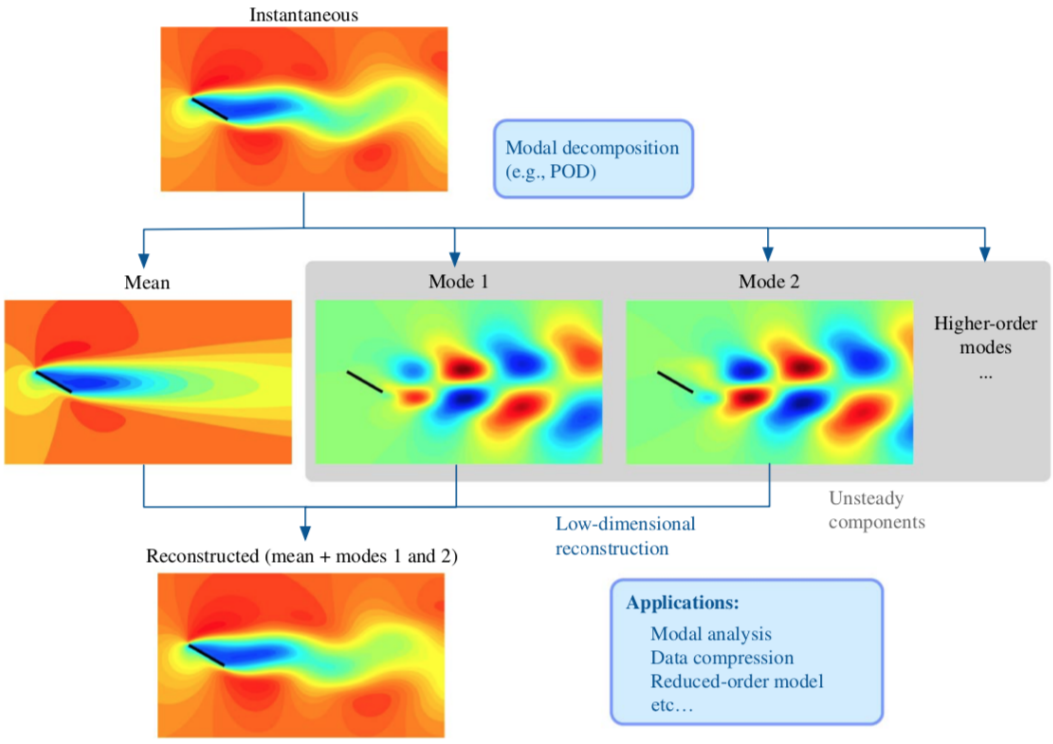

Figure 1.2: Modal decomposition of two-dimensional flow over a flat plate (Re = 100) [11]

The applications mentioned should demonstrate that these methods are well-developed and have the potential to be used as a tool in a variety of flows. However, their use is often limited to analyzing simplified flows or very specific features of complex flows. This research aims to expand our knowledge on the capability of modal decomposition to analyze a flow with a range of intricately involved, unsteady features. An interesting example of such a problem is supersonic flow over a wall-mounted turret, discussed further below. This flow contains a wide variety of complex phenomena, including multiple unsteady shock waves and separated shear layers. These unsteady features cause significant problems for the application of turrets on supersonic airborne aircraft, so characterizing the flow is important for developing control strategies. The goal of this work is to use modal decomposition to extract the dominant features and provide a better understanding of the main features underlying the observed flow unsteadiness. Through this application, the strengths and weaknesses of both DMD and POD will be outlined. The purpose of using both in this research is to highlight how

they complement each other in the analysis of a very complex flow.

1.1.1 Proper Orthogonal Decomposition (POD)

The Proper Orthogonal Decomposition (POD) is a modal decomposition technique which aims to decompose data into a minimal number of basis vectors or modes that contain the most energy in the system over time. The name "proper", or optimal indicates that the mean square distance (or error) between the original signal and the data represented in the lower dimensional POD basis is minimized. The basis vectors extracted are spatially-correlated modes which describe the unsteady variation of the flow variable under examination. This method was introduced to the field of fluid mechanics by Lumley in 1967 [12] as a means of extracting coherent structures in turbulent flows. Once the decomposition is performed, there is an objective way to rank dynamic features based on their addition to the systems total energy.

As an example, when POD is applied to a fluid problem, the starting point is the raw data $\mathbf{U}(\mathbf{x}, t)$ (e.g.,velocity) which was recorded for a fluid domain over a finite number of time steps. This method then defines features in this data based on their contribution to variance or deviation from the mean flow. Thus, we look at the unsteady component of the full domain,

$$\mathbf{U}'(\mathbf{x}, t) = \mathbf{U}(\mathbf{x}, t) - \bar{\mathbf{U}}(\mathbf{x}) \tag{1.1}$$

where $\mathbf{U}(\mathbf{x}, t)$ is the instantaneous value, $\bar{\mathbf{U}}(\mathbf{x}, t)$ is the temporal mean and $\mathbf{U}'(\mathbf{x}, t)$ is the fluctuation. The data is assumed to have the ability to be decomposed in the following superposition:

$$\mathbf{U}'(\mathbf{x}, t) = \sum_{j}^{N} a_j(t)\boldsymbol{\phi}_j(\mathbf{x}) \tag{1.2}$$

where $\boldsymbol{\phi}_j(\mathbf{x})$ are the spatial modes and $a_j(t)$ are the expansion coefficients, which vary with

time. While there are many different variances of the form in equation (1.2), this one is used when there is a desire to extract only spatially dependent modes. The energy of each mode is measured by its contribution to the total variance of the flow field variable being examined [13]. Although fluctuations in flow variables such as pressure or velocity are stochastic in turbulent flows, the POD modes show the existence of some order in those apparently disorganized fields. The modes show, spatially, how those fluctuations are correlated. The time coefficients on the other hand, indicate how the magnitude of those fluctuations change with time. The details on the algorithm which computes these modes and coefficients is outlined in section (2.2).

The POD method is one of the most widely used techniques in studying fluid flows, as the dimension of the problem is often extremely high and requires advanced post-processing techniques before insight to the physics can be gained. Some examples include application to reduced order modeling, data compression, and flow control. There are a variety of applications outside of fluids, including understanding the nonlinear dynamics of structures [14]. It also has had applications in many non-engineering fields, under other names, including Principle Component Analysis (PCA) in statistics and factor analysis in psychology and economics. While the data collected in these fields may seem very different from fluids, they are both unsteady and contain a large number of degrees of freedom, thus lending themselves well to the POD.

The major drawback of this method is that energy is not always the most useful measurement to rank the systems modes. Although POD identifies these energy dominating spatial modes, their time evolution comprises a combination of several frequencies. Furthermore, there may be aspects of the flow that are dynamically important, but are low in energy, such as flows where acoustics or transition to turbulence are of interest. In attempts to address these issues, variants of POD have been developed including Spectral POD (SPOD) [15] and Balanced POD (BPOD) [16]. The SPOD analysis extracts orthonormal modes with discrete

frequencies that are still optimally ranked in terms of energy. The BPOD analysis extracts two sets of modes that are a biorthogonal set and are ranked by controllability/observability. The goal of both variants is to provide more information about the system dynamics, so that important but low energy modes are not truncated. The weaknesses of POD are naturally addressed in the DMD analysis, which focuses on identifying modes at specific frequencies and are of interest in a dynamic (time-varying) sense.

1.1.2 Dynamic Mode Decomposition (DMD)

The Dynamic Mode Decomposition (DMD) is a modal decomposition technique that extracts spatial coherent structures with a single temporal frequency and growth/decay rate. The method was introduced to the fluids community by Schmidt [17], who defined the algorithm and demonstrated its ability to provide insight to fluid data. This method has been said to combine the favorable aspects of both the POD and Fourier transforms with time. Similar to these methods, DMD is relatively easy to implement and makes no assumptions about the underlying dynamics.

Realistic dynamical systems are often governed by partial differential equations that are coupled and nonlinear, with no known analytical solution. In fluid dynamics, these are usually some form of the Navier-Stokes Equations. Generally, when dealing with nonlinear systems, it can be insightful to find an approximate linear solution,

$$\frac{d\mathbf{x}}{dt} = \mathcal{A}x \tag{1.3}$$

with initial condition $x(0)$, where $\mathcal{A}$ is a Jacobian representing the linearization of the original equation set. This equation allows for a solution of the type:

$$\mathbf{x}(t) = \sum_{k=1}^{n} \phi_k \exp\left(\omega_k t\right) b_k = \Phi \exp(\Omega t)\mathbf{b} \tag{1.4}$$

where ϕ_k and ω_k are the eigenvectors and eigenvalues of the matrix $\mathcal{A}$, and the coefficients b_k are the coordinates of $x(0)$ projected onto the eigenvector basis. When the governing equations are as complex as the Navier Stokes, the numerical solution is obtained after discretization. This generates the state of the system sampled every Δt, where $x = x(k\Delta t)$. For a fluid simulation, this is equivalent to recording flowfield snapshots. The discrete time analogy to equation (1.3) is given by:

$$\mathbf{x}_{k+1} = \mathbf{A}\mathbf{x}_k \tag{1.5}$$

where

$$\mathbf{A} = \exp \mathcal{A}\Delta t \tag{1.6}$$

The matrix $\mathbf{A}$ can be thought of as the "best-fit" linear operator that advances a flowfield snapshot one time step into the future. Just as in the continuous time dynamical system, equation (1.5) has an approximate solution,

$$\mathbf{x}_k = \sum_{j=1}^{N} \phi_j \lambda_j^k b_j = \Phi \Lambda^k \mathbf{b} \tag{1.7}$$

where Λ are the eigenvalues and Φ eigenvectors of the linear operator $\mathbf{A}$. The coefficients, $\mathbf{b}$, are computed by projecting the initial snapshot $\mathbf{x}_1$ onto the eigenvector basis. As the data being analyzed is nonlinear, the best linear operator will vary from snapshot to snapshot. The goal is to find the one matrix that optimally fits the measured data so that $\|\mathbf{x}_{k+1} - \mathbf{A}\mathbf{x}_k\|_2$ is minimized over all snapshots ($k = 1, 2, ..., m$). As stated before, the data being analyzed is high dimensional ($N >> 1$). As a result, directly computing $\mathbf{A}$, of size N^2, and its eigendecomposition is not feasible. The DMD algorithm overcomes this by computing a reduced order representation of the linear operator, defined as $\tilde{\mathbf{A}}$, by utilizing a similarity transform and the relevant POD modes. This new low-rank matrix is much smaller and has the same leading eigenvalues of the full-rank matrix $\mathbf{A}$. The full eigenvectors of $\mathbf{A}$, also

known as the DMD modes, are determined by projecting the eigenvectors of $\tilde{\mathbf{A}}$ back into the full domain. The full details of this algorithm are outlined in section (2.4).

It may appear to be a major approximation to represent the results from the nonlinear Navier-Stokes equations with a linear operator; however, it has been shown that DMD is closely related to a spectral analysis of the Koopman operator [18]. This technique represents an infinite-dimensional linear operator whose modes and eigenvalues capture the evolution of any dynamical system, even a nonlinear one. DMD can be thought of as a numerical approximation to the Koopman operator, and thus, is applicable to nonlinear systems.

One of the main weaknesses of the DMD method is the difficulty in finding a sparse number of modes to represent the flow. Truncation with DMD is not as direct as with the POD method because the modes are not spatially orthogonal and there is no objective ranking. As seen in equation (1.7), the modes do have corresponding amplitudes; however, these are based on the initial condition. Unlike POD, the largest amplitude DMD modes may not have the strongest impact on the overall flow dynamics. To address this issue, a variant called Sparsity Promoting DMD (SPDMD) was developed [19]. This method aims to achieve a desirable trade off between quality of approximation and the number of modes used to reconstruct the flow. A deeper knowledge of the system under examination can also aid in the identification of important modes. For example, if the frequencies of interest are known, the modes associated with those dynamics can be easily extracted and visualized.

This method thus addresses one of the main issues of POD, as it has the ability to study features of a flowfield at specific frequencies and does not truncate based on a modes energy content. Instead of extracting the dynamic modes that are important purely from an energy perspective, DMD constructs an approximate linear flow solution and captures features that are seen as dynamically important.

1.2 Supersonic Flow Over a Wall-Mounted Turret

This research aims to expand our knowledge on how modal decomposition can be used as a tool to study fluid problems with a variety of complex features, as well as provide useful information for developing flow control strategies. An interesting example of such a problem is supersonic flow over a wall-mounted protuberance, such as a turret on an aircraft. Hemispherical turrets are optimal platforms for projecting and receiving laser beams due to their large field-of-view. When placed on airborne vehicles moving at transonic to supersonic speeds, the flow-physics become unsteady and complicated. The features that evolve, including multiple shock waves and regions of separation, cause distorting aero-optic effects on the laser projected from the turret. There has been extensive computational and experimental research in the subsonic and transonic regimes for this flow; however, because the unsteadiness and complexity of the physics increase in intensity with Mach number, the supersonic regime has gone widely unstudied. As a result, the application of these laser systems has seemed impractical for supersonic aircraft. Recent advances in high-fidelity computations, however, have greatly improved the ability of simulating this type of flow and resolving the complex flow features. Extensive effort has been put into developing simulations for supersonic flow over wall-mounted protuberances using RANS, hybrid RANS/LES, DDES, and LES based models. The simulations have advanced from forward facing cylindrical steps [20] and wall-mounted half-cylinders [21], to full wall-mounted hemispheres [22, 23]. The high-order implicit LES based models have shown good agreement with subsonic experiments. While there is a lack of extensive published experimental data in the high-speed regime, there is adequate confidence in the data because of their high-fidelity underlying algorithms. The high-dimensional data that results from this type of simulation thus lends itself well to be analyzed using modal decomposition.

1.2.1 Flow physics description

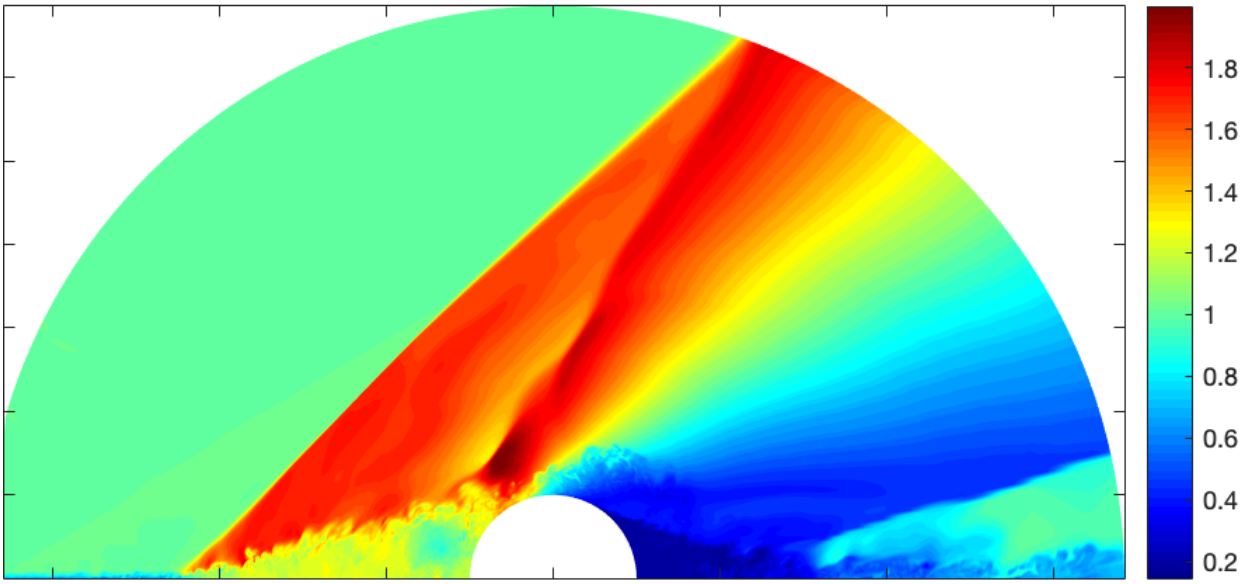

Figure 1.3: Instantaneous snapshot of flowfield density

The dataset analyzed in this research is Mach 2 flow over a wall-mounted turret. Specifically, the turret was approximated with a spanwise homogeneous wall-mounted half cylinder. An instantaneous snapshot of the flowfield density from this simulation is shown in figure 1.3. A similar Mach 2 simulation was performed in reference [21] over the same geometry. For reference, a detailed description of the mean flow characteristics from their simulation can be seen in figure 1.4.

The flow is moving from left to right. An incoming turbulent boundary layer develops upstream of the cylindrical body. This interacts with the cylinder and forms a subsonic separation region near the surface. At the edge of this separation bubble, a separation shock forms. The interaction of this shock with the turbulent boundary layer results in its unsteady motion. A shear layer develops downstream of this interaction, which impinges on the cylinder forming an unsteady recirculating region. The flow accelerates over the cylinder and then forms another unsteady separation region on the aft side of the cylinder. This leads to a shear layer impinging on the flat plate which generates an additional unsteady

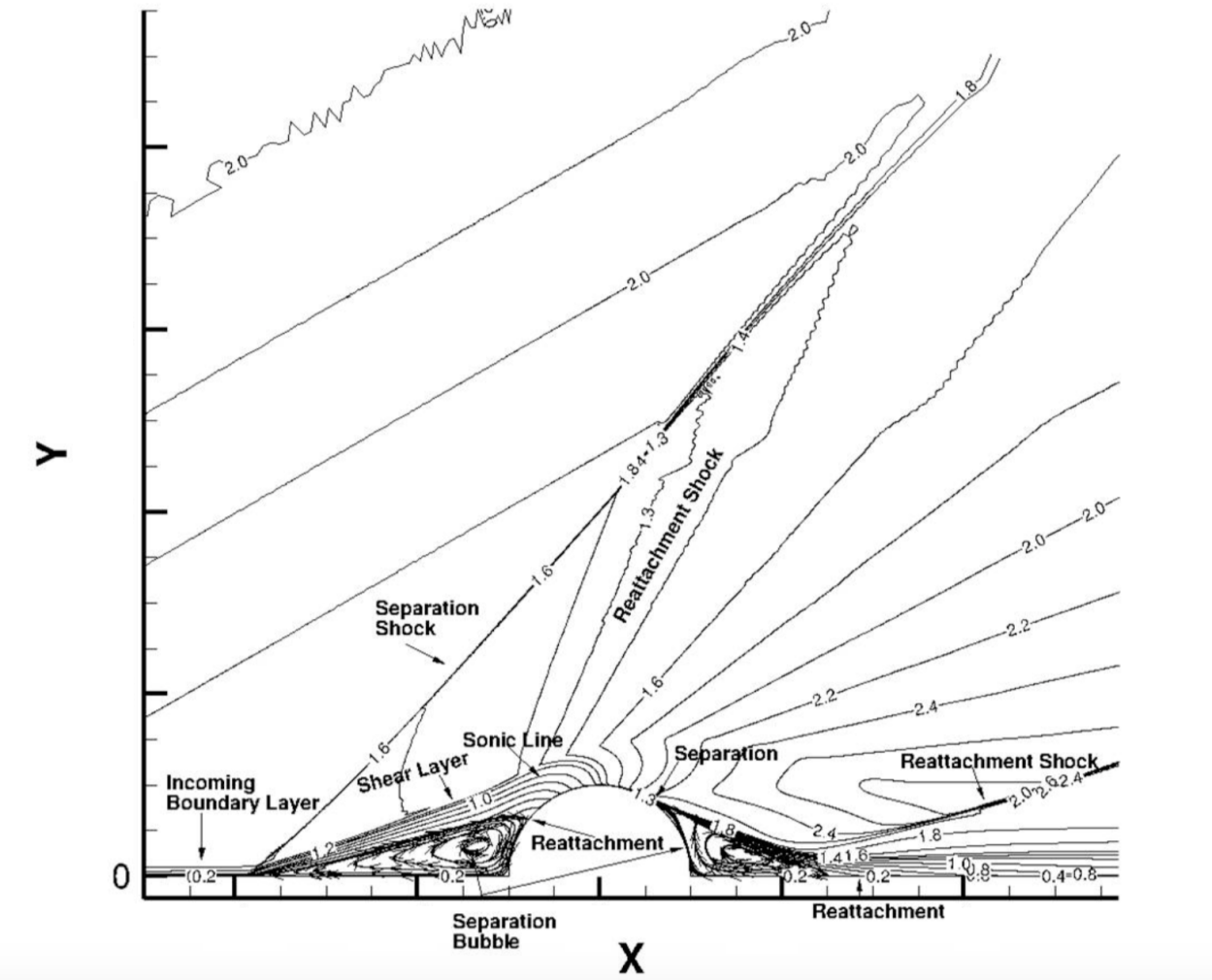

Figure 1.4: Streamlines describing unsteady features in supersonic flow past a wall-mounted cylinder from ref. [21]

reattachment shock. This third shock wave is much weaker than the two in front of the cylinder. The sonic line resides near the top of both the upstream and downstream shear layers.

It should be noted that the features found in this 2D turret representation are different than those that appear in the fully 3D flow. For reference, a schematic of the unsteady features found in supersonic flow around a hemispherical turret can be found in figure 1.5 from reference [24]. One of main the differences is the absence of the necklace vortex in the 2D flow, due to it being spanwise homogeneous. In addition, the 3D flow contains a detached

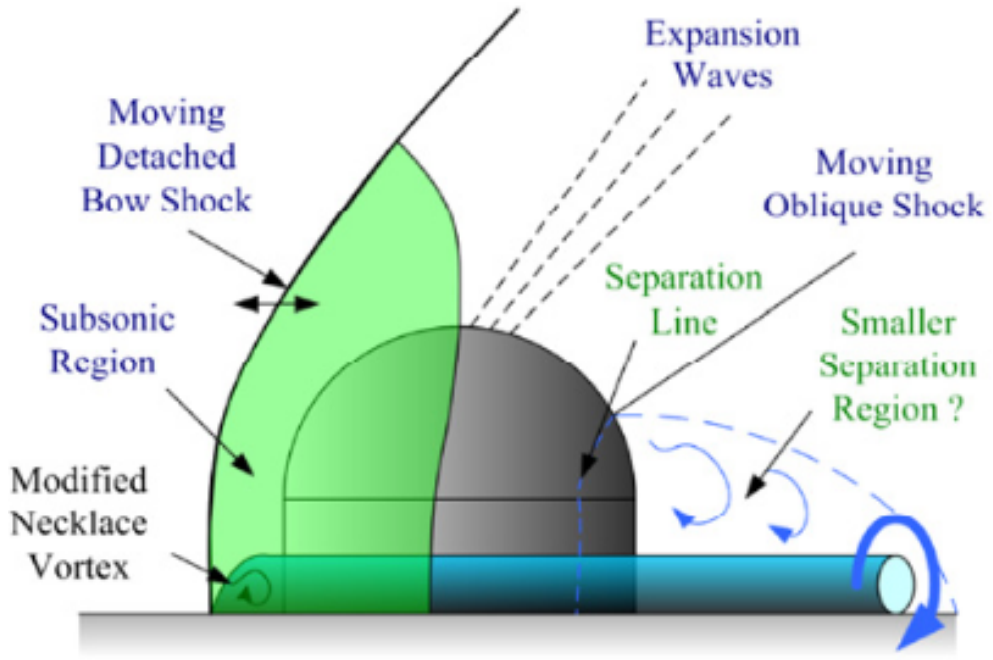

Figure 1.5: Schematic of unsteady features in supersonic flow around a turret [24]

bow-shock, analogous to the separation shock found in the 2D flow. However, both of these leading shock waves are unsteady due to interactions with the turbulent boundary layer on the wall. In addition, both flows have unsteady oblique shocks and separated shear layers near the surface of the turret. These similar unsteady features make this nominally 2D flow a good approximation for analyzing this problem using modal decomposition.

The unsteady phenomena seen in this flow impose effects that distort the optics of the laser beam projected from an airborne turret. For example, the shocks and expansion waves introduce large density gradients in the flow near the turret which ultimately results in aero-optically induced jitter. The interaction between the shock-waves and turbulent boundary layer results in larger separation regions. The large unsteady pressure and velocity fluctuations result in unsteady forcing of the turret structure [23]. This leads to mechanically induced jitter disturbances. As speed increases, the intensity of these effects increase [24]. Finding flow control strategies is critical for these turrets to ever be used in supersonic applications.

1.2.2 Application of Modal Decomposition

As discussed, the flow past a wall-mounted cylinder contains a variety of unsteady features. The coherent structures that arise due to these phenomena are diverse, multiscale, and broadband. The complex nature of this flow lends itself well to be analyzed using modal decomposition. As the techniques separate modes based on characteristics like total fluctuation and frequency, the various features of this flow should be able to be separately extracted and characterized.

As noted earlier, the POD method objectively characterizes modes based on their contribution to the overall unsteadiness in the flow. This technique will be used to capture the dominant large-scale coherent structures and quantify the energy content; thus, impartially ranking features that are dominating the unsteadiness. The DMD method extracts modes that approximate the dynamics present in the data, with each accompanied by a characteristic frequency. This technique will be used to capture structures that are evolving at the same frequency, ensuring they are being characterized based on dynamics. Together, these methods will be used to detail the unsteadiness and dynamics of the dominant coherent structures, which is important for developing control strategies that will target those features.

Although this flow is complex in nature, many of the features within the problem have been widely studied individually. For example, the unsteady shock waves impose strong density gradients that complicate the performance of turret-based lasers. These shocks move due to their interaction with the turbulent boundary layer which develops both on the wall upstream of the turret and on the turret itself. In fundamental analysis of shock wave/turbulent boundary layer interactions (SWTBLI), there is a characteristic low-frequency associated with the interaction. This frequency has been shown to scale with free stream velocity and separation length [25], designated a Strouhal number, $St_{L_{sep}} = \frac{fL_{sep}}{U_\infty}$. The frequency range

is well accepted to be between $0.03 < St_L < 0.5$. In addition, the turbulent boundary layer that develops upstream of the first separation shock has a frequency content about two orders of magnitude higher than those associated with the shock. The POD analysis will be used to quantify how these shocks contribute to the unsteadiness compared to the other features. The DMD analysis will be used to decompose the features into their characteristic frequencies. The low frequency range will be targeted to see if the dynamics of the unsteady shock waves can be identified. The details of these dynamics will allow for the SWTBLI in this flow to be better characterized and for flow control techniques can be developed.

This analysis will allow you to objectively quantify the energy content of each flow feature and provide detail about the dynamics, which is pivotal for developing effective control strategies. The strengths and weaknesses of each will be outlined in order to paint the picture of how they compliment each other in the analysis of the complex problem at hand. In Chapter 3, the unsteady turret flow will be decomposed and analyzed using both techniques with the goal of providing details about the dynamics of the main flow features.

Chapter 2: Methods

2.1 Data Format Description

The modal decomposition techniques used in this work require only flowfield data, in the form of snapshots, as input to the analysis. The data analyzed was obtained at the High-Fidelity Computational Multi-Physics Lab (HFCMPL) from Large Eddy Simulations (LES). The total size of the spatial dimensions, $N_{3D} = 1772 \times 709 \times = 8,794,436$. The snapshots comprise 2-D planes normal to the axis of the cylinder, each containing $N = 1772 \times 709$ data points of the five quantities, density (ρ), streamwise (u), plate-normal (v) and spanwise (w) velocities, and pressure (p).

The temporal dimension comprises the number of snapshots and is denoted as M. In the present case, a total of 7000 snapshots were considered, so $M << N$. For the vector field of interest to be decomposed, the data must be reordered from its original 3D format. For each time instant t_k, we concatenate the individual snapshots into one single $N \times 1$ column. The different time-step snapshots are then stacked as columns to form a snapshot matrix. For example, if the data of interest is the flow field velocity, the $N \times M$ snapshot matrix U is as follows,

$$\mathbf{U} = \begin{pmatrix} u_{11} & \dots & u_{1M} \\ u_{21} & \dots & u_{2M} \\ \vdots & & \vdots \\ u_{N1} & \dots & u_{NM} \end{pmatrix} = \begin{pmatrix} u\left(x_1, y_1, t_1\right) & \dots & u\left(x_1, y_1, t_M\right) \\ u\left(x_2, y_2, t_1\right) & \dots & u\left(x_2, y_2, t_M\right) \\ \vdots & \vdots & \vdots \\ u\left(x_{Nx}, y_{Ny}, t_1\right) & \dots & u\left(x_{Nx}, y_{Ny}, t_M\right) \end{pmatrix} \tag{2.1}$$

Once the data is in this form, the decomposition can be performed through different ways of matrix analysis. Once the modes are obtained, the data is "unstacked" back into its original

format in like fashion for visualization and analysis of the decomposed modes.

2.2 Proper Orthogonal Decomposition

Although the mathematical theory and error analysis underlying POD is very sophisticated, the implementation is relatively simple due to the fact that it is essentially a matrix-based procedure. An overview of the POD approach was provided in Chapter 1. The initial step, as noted there, is to consider a variable of interest, such as velocity $\mathbf{U}(\mathbf{x}, t)$, which is a function of both space, $\mathbf{x} = (x, y, z)$, and time, t. It is typical to write this variable in terms of its unsteady component or fluctuations,

$$\mathbf{U}'(\mathbf{x}, t) = \mathbf{U}(\mathbf{x}, t) - \bar{\mathbf{U}}(\mathbf{x}) \tag{2.2}$$

where $\bar{U}$ is the temporal mean of the velocity field. The data is formatted into a snapshot matrix as described in equation (2.1), resulting in an $N \times M$ snapshot matrix of fluctuations as follows,

$$\mathbf{U}' = \begin{pmatrix} u'(x_1, y_1, t_1) & \dots & u'(x_1, y_1, t_M) \\ u'(x_2, y_2, t_1) & \dots & u'(x_2, y_2, t_M) \\ \vdots & \vdots & \vdots \\ u'(x_{Nx}, y_{Ny}, t_1) & \dots & u'(x_{Nx}, y_{Ny}, t_M) \end{pmatrix} \tag{2.3}$$

This unsteady component is then decomposed into a set of deterministic spatial functions, or POD modes, regulated by time coefficients in the following manner,

$$\boldsymbol{U}'(\mathbf{x}, t) = \sum_{k=1}^{N} a_k(t) \boldsymbol{\Phi}_k(\mathbf{x}) \tag{2.4}$$

where $\boldsymbol{\Phi}_k$ are the POD (spatial) modes and $a_k(t)$ are the corresponding time coefficients.

There are multiple techniques for decomposing the data in such a manner. The direct POD method can be computationally intensive for problems with large spatial dimensions, as it involves solving an eigenvalue problem of size $N \times N$. The technique employed in this project is called the method of snapshots, which has been found to be much more efficient than the direct solution [26], as it solves an eigenvalue problem based on the size of the time dimension, $M \times M$.

The POD modes are computed by finding the optimal basis that represents the given data. The optimality is in the least-squares sense, which minimizes the number of modes required to describe the signal for any given error. The solution is determined by solving for the eigenvalues and eigenvectors from,

$$\boldsymbol{C}\boldsymbol{\Psi} = \lambda\boldsymbol{\Psi} \tag{2.5}$$

where $\boldsymbol{C}$ is the covariance matrix of $\boldsymbol{U}'(\mathbf{x}, t)$, which for the snapshot method is defined as,

$$\boldsymbol{C} = \frac{1}{M-1} U^T U \tag{2.6}$$

The result is an $M \times M$ (square) matrix, which considers the correlation between different data points *i.e.,* how they 'move' together. Since the variance is taken over the time dimension, the eigenvectors extracted, Ψ, are the temporal modes. In order to get the spatial modes and temporal coefficients, which would be the result of the direct POD method, the data must be projected back into the full N-dimensional space and normalized,

$$\boldsymbol{\Phi} = \frac{\mathbf{U}'\boldsymbol{\Psi}}{\sqrt{\lambda}} \tag{2.7}$$

$$\mathbf{A} = \mathbf{U}'^{\mathbf{T}}\boldsymbol{\Phi} \tag{2.8}$$

where the columns of $\boldsymbol{\Phi}$ are the spatial POD modes and the rows of $\mathbf{A}$ contain the corresponding temporal coefficients.

With the spatial modes and time coefficients computed, the data can then be fully reconstructed by using equation (2.4) and adding back the mean flow. At this point, however, the dimension of the problem can be reduced by truncating the modes based on percent of total energy. Reconsidering equation (2.5), the eigenvalues extracted from the covariance matrix are a measure of time-averaged energy and are then used to rank the modes from strongest to weakest. Deciding when to truncate is based on judgement, though there are more objective approaches that have been proposed. For this research, mode truncation and flowfield reconstruction were not of interest, since the main focus is on using this method as a means of objectively ranking the flow features based on their energy, or contribution to the total variance of the flow variables.

2.3 Singular Value Decomposition

Although it was not used in this research for the POD analysis, many algorithms utilize the Singular Value Decomposition (SVD) to solve for the POD modes and corresponding eigenvalues or singular values. The snapshot method was used in this research because it is simple and provides the best clarity on the mechanics of the decomposition. However, understanding how the SVD is connected to POD is important, as it is used in the development of the DMD algorithm subsequently. For clarity, it is described in this section.

The POD method described in the previous section is equivalent to the SVD of matrix $U'/\sqrt{m-1}$. Taking the SVD of this matrix would decompose as follows,

$$\mathbf{U}' = \mathbf{L}\mathbf{\Sigma}\mathbf{R}^T \tag{2.9}$$

where the columns of $\mathbf{L}$ are the left singular vectors, the diagonal elements of Σ are the singular values, and the columns of $\mathbf{R}$ are the right singular vectors. Assuming the data

matrix is stacked with the full snapshots in columns, the left singular vectors span the spatial dimension and the right singular vectors span the temporal dimension. Thus, the POD spatial modes are easily extracted. In addition, the square of the singular values are equal to the eigenvalues in equation (2.5). The SVD method is used to find the POD modes in the DMD algorithm, outlined in Chapter 3. The theory behind SVD is discussed extensively in linear algebra and matrix math textbooks [27].

2.4 Dynamic Mode Decomposition

Similar to the POD method, DMD describes the flow as a combination of correlated spatial modes; however, these modes are associated with a given temporal frequency, possibly with a growth or decay rate. There are many variations of the direct DMD algorithm; each designed to leverage desired features of interest. The algorithm followed in this research was found in the DMD textbook on data driven modeling [7].

To begin, two snapshot matrices must be constructed, with the same format as described in equation (2.1), stacked into an $N \times M$ matrix, shifted one time step apart from each other as follows,

$$\mathbf{X} = \begin{bmatrix} | & | & & | \\ \mathbf{x}_1 & \mathbf{x}_2 & \cdots & \mathbf{x}_{M-1} \\ | & | & & | \end{bmatrix} \tag{2.10}$$

$$\mathbf{X}' = \begin{bmatrix} | & | & & | \\ \mathbf{x}_2 & \mathbf{x}_3 & \cdots & \mathbf{x}_{M} \\ | & | & & | \end{bmatrix} \tag{2.11}$$

The locally linear approximation of the nonlinear data may be written as,

$$\mathbf{X}' \approx \mathbf{A}\mathbf{X} \tag{2.12}$$

where $\mathbf{A}$ is the best-fit linear operator for all snapshots, that maps $\mathbf{X}$ to $\mathbf{X}'$. To solve for $\mathbf{A}$, the psuedoinverse of $\mathbf{X}$ is taken,

$$\mathbf{A} = \mathbf{X}'\mathbf{X}^{\dagger} \tag{2.13}$$

The psuedoinverse computes the "best-fit" inverse of $\mathbf{X}$, as the direct inverse cannot be taken for the rectangular matrix. DMD is interested in finding the leading eigenvalues and eigenvectors of this matrix $\mathbf{A}$. If computed directly, the result is an $N \times N$ matrix, which would require an eigenvalue problem of size $N \times N$. In general, the dimension of fluids data is very large, so the matrix $\mathbf{A}$ can become intractable to compute directly for typical high-fidelity simulations. In addition, the rank of the data matrix $\mathbf{X}$ is at most $(M-1)$, as it was constructed as a linear combination of $(M-1)$ snapshots. Thus, computing the full $N \times N$ $\mathbf{A}$ matrix does not actually provide more information and a rank truncation can greatly alleviate the computational difficulty.

The Singular Value Decomposition (SVD) of the matrix $\mathbf{X}$ may be written as,

$$\mathbf{X} \approx \mathbf{U}\Sigma\mathbf{V}^{*} \tag{2.14}$$

where $*$ identifies the conjugate transpose. The sizes of the different matrices are: $\mathbf{U} \in \mathbb{C}^{N\times(M-1)}$, $\Sigma \in \mathbb{C}^{(M-1)\times(M-1)}$, and $\mathbf{V}^{*} \in \mathbb{C}^{(M-1)\times(M-1)}$. This method is called the economy size or reduced SVD, as the rank is reduced from N to $M-1$. The columns of $\mathbf{U}$ are POD modes which, as stated previously, are orthonormal and the ideal basis to represent the data. To avoid analyzing the large-dimension $\mathbf{A}$ matrix, DMD utilizes the properties of a similarity

transform and projects it onto the POD modes to form low-rank approximation matrix, $\tilde{\mathbf{A}}$.

$$\begin{aligned}\tilde{\mathbf{A}} &= \mathbf{U}^{\star}\mathbf{A}\mathbf{U} \\ &= \mathbf{U}^{\star}\mathbf{X}'\mathbf{V}\boldsymbol{\Sigma}^{-1}\end{aligned} \tag{2.15}$$

Just as $\mathbf{A}$ is a linear model of the evolution of the system in the $N-$dimensional space, $\tilde{\mathbf{A}}$ is a linear model which describes the evolution of the system in the $(M-1)-$dimensional POD coordinates.

$$\tilde{\mathbf{x}}_{k+1} = \tilde{\mathbf{A}}\tilde{\mathbf{x}}_k \tag{2.16}$$

Since this low-dimensional model was constructed using a similarity transform, the leading eigenvalues are identical to the full-dimensional model. Thus, the eigendecomposition on $\tilde{\mathbf{A}}$ is computed.

$$\tilde{\mathbf{A}}\mathbf{W} = \mathbf{W}\boldsymbol{\Lambda} \tag{2.17}$$

where columns of $\mathbf{W}$ are eigenvectors and the diagonal entries of $\boldsymbol{\Lambda}$ contain the corresponding eigenvalues.

These matrices are then used to reconstruct the relevant part of the eigendecomposition of the full $\mathbf{A}$ matrix. The eigenvalues of $\mathbf{A}$ are given by $\boldsymbol{\Lambda}$ and the eigenvectors, $\boldsymbol{\Phi}$, are constructed by projecting $\mathbf{W}$ back onto full high-dimensional domain,

$$\boldsymbol{\Phi} = \mathbf{X}'\mathbf{V}\boldsymbol{\Sigma}^{-1}\mathbf{W} \tag{2.18}$$

The modes in equation (2.18) are referred to as exact DMD modes, as they have been proven to be the exact eigenvectors of the full matrix $\mathbf{A}$ [28]. The eigenvalues, λ, can be scaled to

obtain the frequency and growth rate of each mode as,

$$\omega = \frac{\log(\lambda)}{\Delta t} \tag{2.19}$$

where the imaginary and real parts of ω are the frequency and growth rates respectively. The eigenvalues and DMD modes can then be used to reconstruct the solution at all time-steps.

$$\mathbf{x}(t) \approx \sum_{k=1}^{r} \boldsymbol{\phi}_k \exp\left(\omega_k t\right) b_k = \boldsymbol{\Phi} \exp(\boldsymbol{\Omega} t)\mathbf{b} \tag{2.20}$$

where $\omega_k = \ln \lambda_k / \Delta t$, b_k is the initial amplitude of each mode, and $\boldsymbol{\phi}_k$ are the DMD modes.

Similar to the POD analysis, there is a separation between the temporal and spatial dimensions. While the time dynamics can be computed, for a statistically stationary flow the growth rates are zero (within numerical error) and the magnitudes oscillate with the frequency. A more revealing approach is to plot the modes and examine the corresponding frequency. The vector lengths of the modes $\boldsymbol{\phi}_k$ are the same as the original state (columns of $\mathbf{X}$) and can be easily visualized by converting back to plotting format.

Chapter 3: Results

3.1 Database description

The LES of supersonic flow over a (2D) turret was performed prior to the start of this project at the Ohio State University. The flow geometry is a wall-mounted half cylinder. For this application, the data under examination is a 2D computational plane cut through the flowfield center z-plane. The flow Mach number is $M_\infty = 2$ and Reynolds number is $Re = 16,209$. The reference conditions were set at $T_{ref} = 162K$, $P_{ref} = 23500Pa$. The reference length used was the incoming turbulent boundary layer height, $\delta = 0.7mm$. All lengths were also scaled by δ. The cylinder radius was set at 10δ. The nondimensional time is defined as $t^* = \frac{tu_{ref}}{L_{ref}}$. The flowfield snapshots were taken every 100 time steps, which resulted in $dt_{snapshot} = 0.1$.

3.2 Convergence Validation

The density and velocity field were used for the basis of the analysis. As noted earlier, $7,000$ snapshots were available, each separated $dt^* = 0.1$. The data was split into windows before it was decomposed, and the results subsequently averaged, to both reduce noise in the DMD spectral analysis and make the computation more efficient. For each window, the data was decomposed into both DMD and POD modes. The dominant mode structures, energy content, and dynamic information was compared over each window. This served as a validation step to check that there was consistency over each window. Specifically, for the DMD analysis, the number of snapshots used in each window was chosen based on

convergence of the frequency for the primary modes, around a consistent number and distinct mode shapes were observed. Similarly, the number of snapshots used in each window for the POD analysis was chosen based on when the energy content for each mode began to converge. It was found that about $2,000$ snapshots were sufficient for both the POD and DMD analysis, which resulted in 6 different windows available for mode, frequency, and energy content comparison.

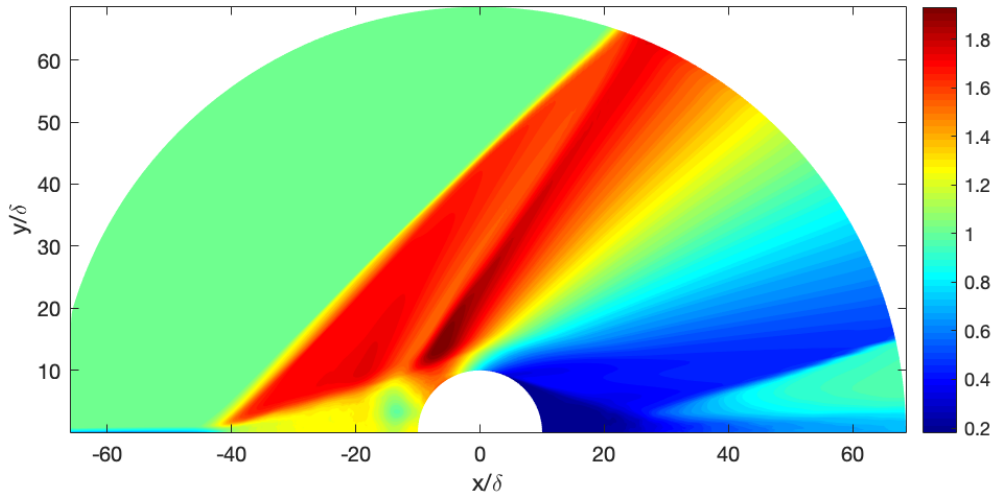

Figure 3.1: Density mean flow

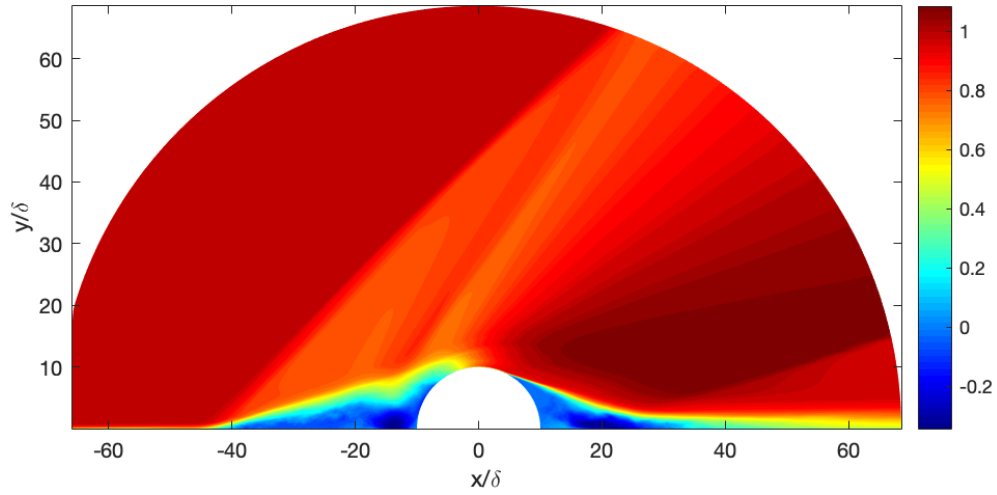

Figure 3.2: Streamwise velocity mean flow

3.3 POD Results

To begin the POD analysis, the temporal mean was subtracted from the flow before decomposition. For reference, the density and velocity mean flow can be seen in figures 3.1 and 3.2. The snapshot matrices were then individually decomposed and the energy distribution per mode was analyzed. It was also important to examine the number of modes required to reconstruct the flow to almost 100% of the total energy, as this is an indicator of the flow dimensionality in the sense of its rank behavior. This objective ranking provided a clear process to selecting which modes to analyze first, focusing on those that contain the most important coherent structures, as observed in the most energetic modes.

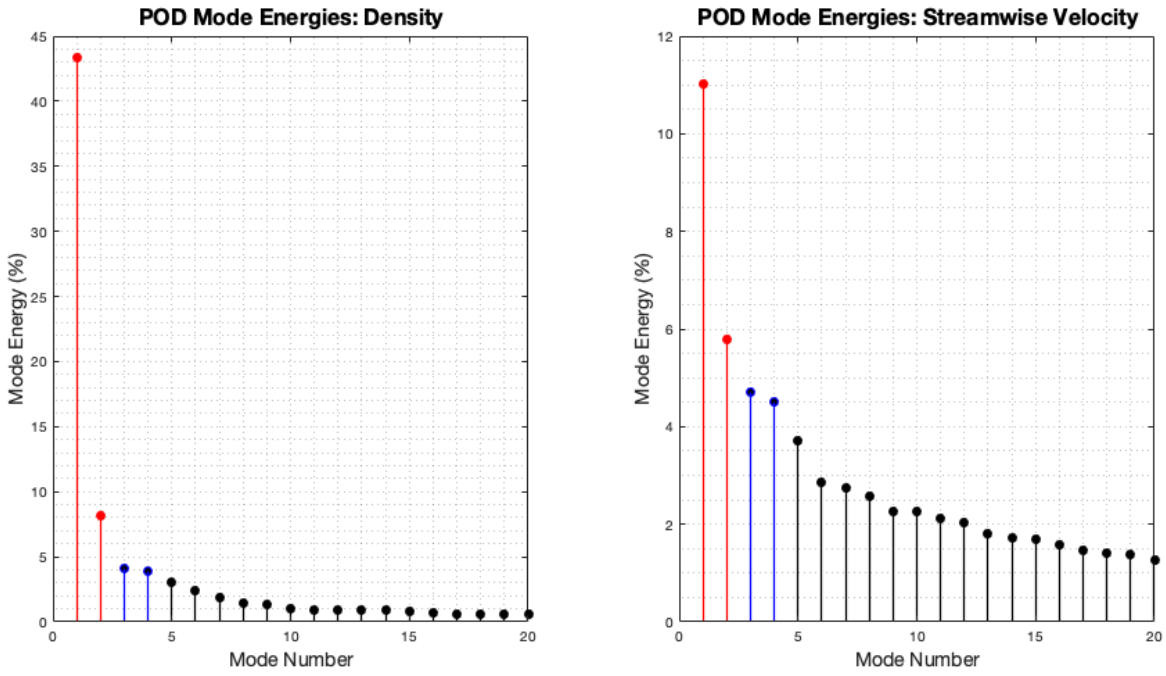

Figure 3.3: Density and streamwise velocity POD mode energies

Figure 3.3 displays the energy distribution per POD mode for the flowfield density and streamwise velocity. It is important to remember that energy is a measurement of how each mode contributes to the total fluctuation of the variable under examination. For the

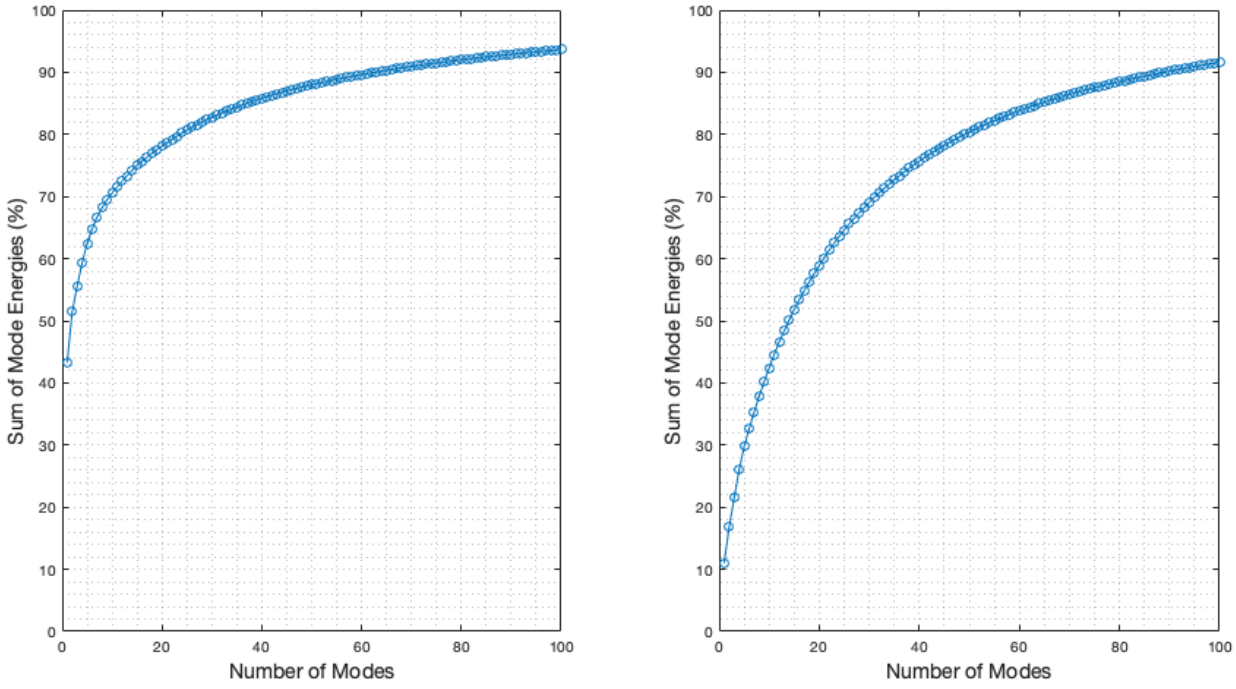

Figure 3.4: Density and streamwise velocity fluctuations, sum of POD mode energies

flow density, the energy distribution is very heavily weighted within the first few modes, as the first mode contains almost 45% of the total energy. For the streamwise velocity, the energy content is still relatively high within the first few modes; however, there is a more even distribution. At first glance, these graphs suggest that a large amount of the density and velocity variation is contained in the first few modes. Figure 3.4 shows the cumulative energy versus number of modes for density and streamwise velocity. Each curve rises rapidly, indicating the prominence of the first few modes, before tapering off as additional modes are considered. Almost 90% of the energy, or variation, is captured in about 100 modes for both variables. This implies that while there is a variety of complicated unsteady features in this flow, there are dominant low-dimensional dynamics dictating most of the density and velocity variation. While energy can be an indicator of how important the mode is to the dynamical system, further analysis of the mode shapes is required to visualize where this energy is being attributed.

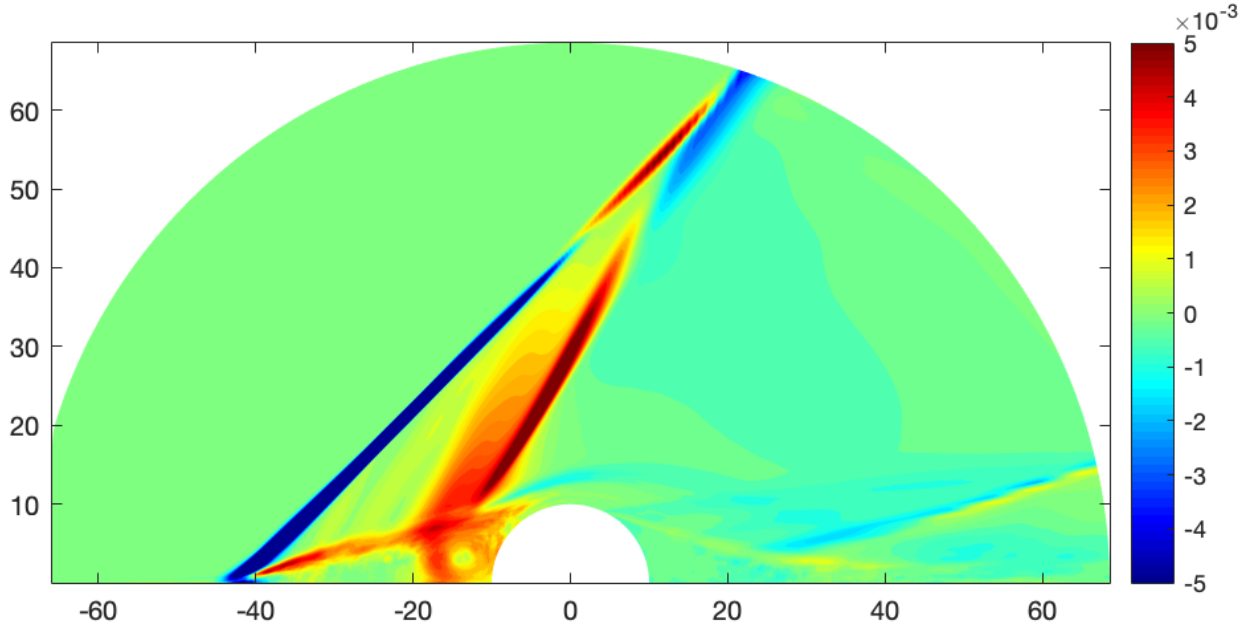

Figure 3.5: Density field fluctuations, first POD mode associated with shock motion, energy $\sim 45\%$

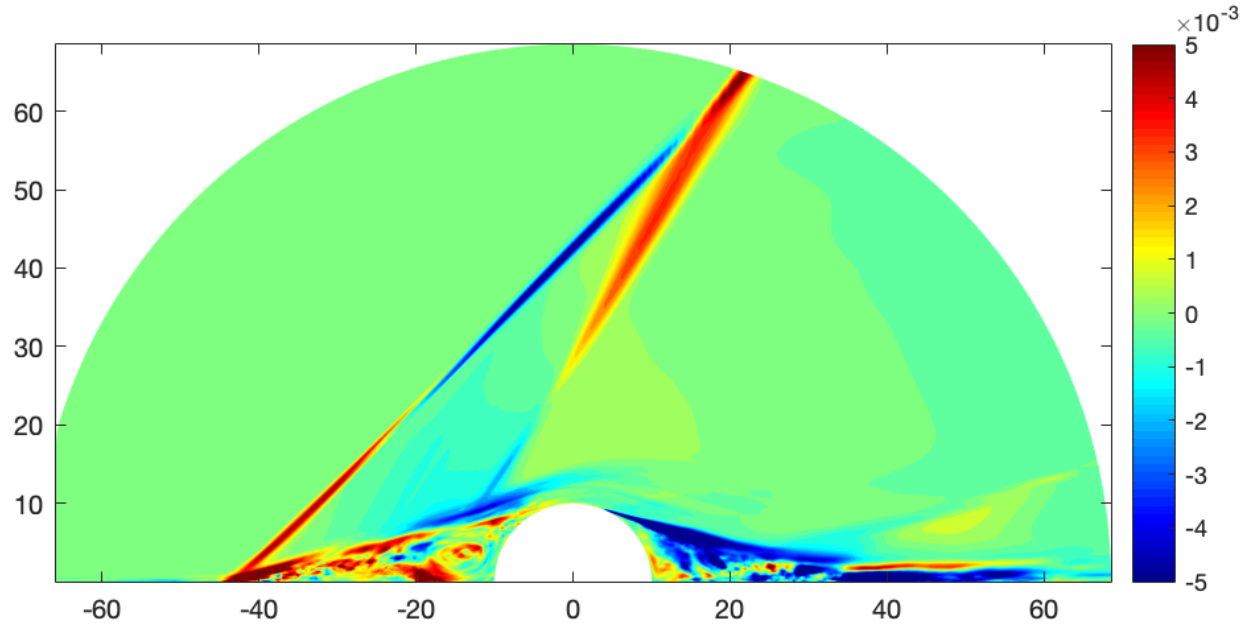

Figure 3.6: Streamwise velocity field fluctuations, first POD mode associated with shock motion, energy $\sim 11\%$

The first density POD mode is shown in figure 3.5. It is clear from this mode shape that it is associated with the variations caused by both the separation and reattachment shocks. A distinct phase difference is evident between the two primary shocks that extend to the farfield. Furthermore, an examination of the magnitude in the shock regions, reveals the interesting fact that the top and bottom of each shock are out of phase with each other.

The upstream shear layer also appears as a feature of high magnitude, which suggests that this mode is also highlighted its interaction with the reattachment shock. The separation shock overall has a higher magnitude along its length, which suggests that it contributes more variance than the second reattachment shock. Nonetheless, together these shocks contribute more than 40% of the density variance in the system. This is important since one of the main problems for the turret application is lasers distortion due the large density fluctuations in the flow.

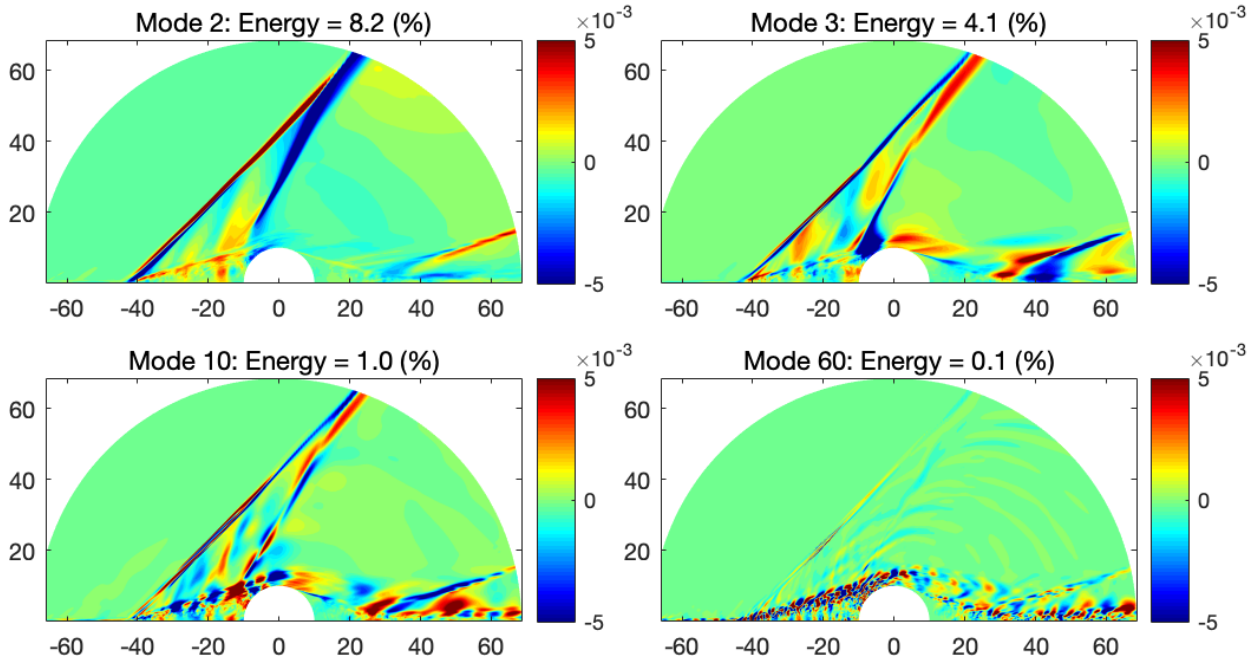

Figure 3.7: Higher-order Density POD modes

The first streamwise-velocity POD mode is shown in figure 3.6. Similar to the density

mode, this figure clearly highlights both the separation and reattachment shocks and the fact that they are moving out of phase with each other. However, now the areas that are of the highest magnitude are the separation regions upstream and downstream of the turret structure. Since the POD modes highlights areas of the flow that are moving or varying together, this suggests that the highlighted regions are influenced directly by the oscillating shock waves.

While the first mode provides important details about the most energetic structures in the flow, it does not reveal the full picture of the system dynamics. Because the shock waves cause the strongest variations in density, the less dominant, but nonetheless crucial features in the rest of the flow are effectively suppressed in the dominant POD mode. That is, it is not the case that the only important features in this flow are the two leading shock-waves, rather, that they are merely the most powerful from an energy perspective. To highlight how the shocks dominate the other features in the POD analysis, higher density POD modes are shown in figure 3.7. Modes 1 and 2 are dominated by the shock waves, while also highlighting areas where larger fluctuations occur. By mode 10, however, although the shock waves are still present, smaller fluctuations around the turret become more apparent. In even higher order modes, as seen in mode 60, the shock structures are not visible and oscillation patterns in the turbulent boundary layer and shear layers become the dominant structures. Once these modes are reached, the energy content has dramatically reduced to less than 1%. This highlights a major weakness in the POD analysis, as the shock waves are the strongest feature in the flow but are not necessarily the only features dictating the unsteady dynamics. While it is important to know that the shocks generate the largest fluctuations, its also vital to understand the other unsteady features in the flow. This goal can be achieved by DMD analysis.

3.4 DMD Results

The modes extracted from DMD are associated with a non-dimensional frequency, which is designated by the Strouhal number, $St_L = \frac{fL_{ref}}{U_{ref}}$. The values of L_{ref} and U_{ref} need not be the same as those used to non-dimensionalize the Navier-Stokes equations. It is often helpful to employ other values that provide better insight. In the case of two-dimensional SWTBLI, the use of the separation length for L_{ref} has proven beneficial because it helps to scale results from different Mach and Reynolds numbers. One possible reason for this is that L_{ref} best represents the strength of the interaction. In the present case, several obvious choices exist, including the incoming boundary layer thickness, δ, the cylinder diameter or the length of the separation region behind the first separation shock. This last quantity is the closest to the separation length in 2-D SWTBLI, and is thus employed here; its value is 17δ. With $2,000$ snapshots used for the decomposition, the frequency spectrum has a range of Strouhal numbers from about 0.3 to 500. Although the DMD method also associates each mode with a growth or decay rate, this flow is statistically stationary which results in those rates being close to zero within numerical error. Once the DMD method is applied to the data, the modes corresponding to the frequencies of interest are identified and compared.

The frequency spectrum for $2,000$ density DMD modes is shown in figure 3.8. For both the density and velocity fields, the lowest frequency mode extracted is always $St_L \sim 0.3$. This mode, as seen in figure 3.8, was almost an order of magnitude lower than the next extracted mode. This mode was of interest because the frequency associated with shock boundary layer interaction is broadly accepted to be low frequency and orders of magnitude lower than those associated with turbulent structures in the flow. The other modes of interest were ones that contained larger structures, such as oscillations in the shear layer and separation regions. The exact frequencies of these types of structures are not known ahead of time since an FFT was not performed; however, it was expected that as the frequency is increased, the size of

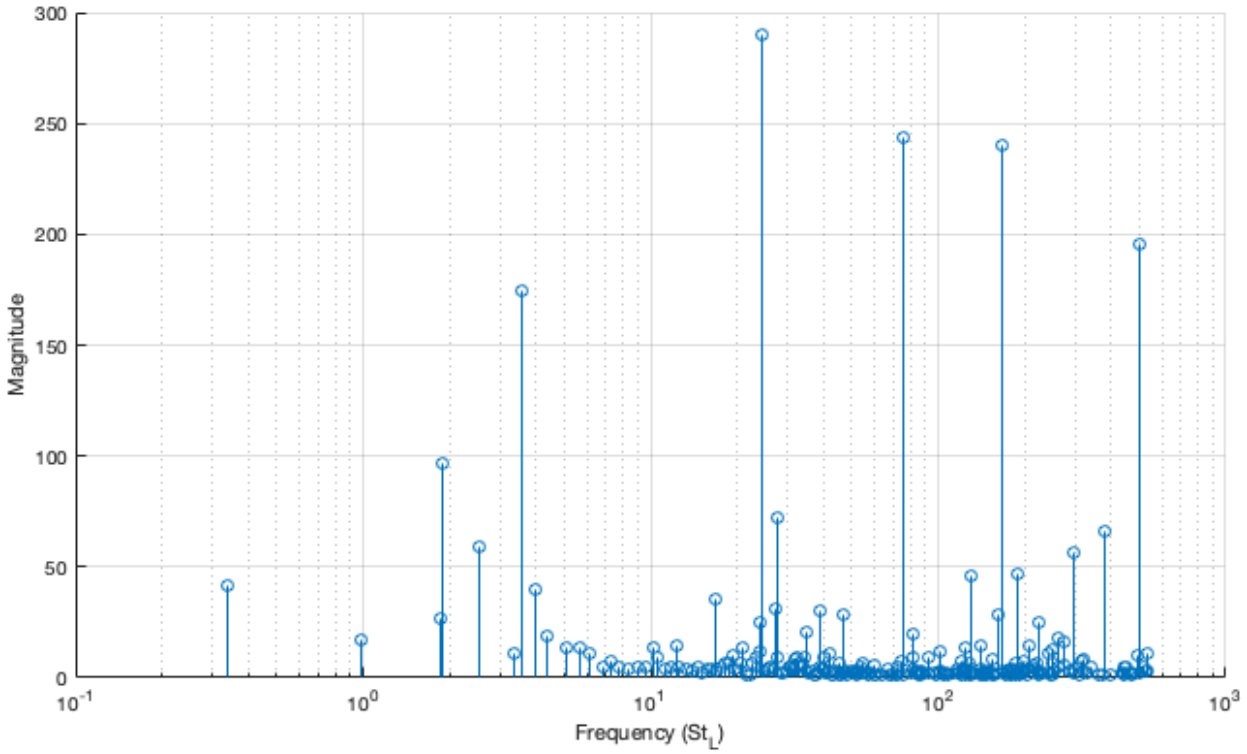

Figure 3.8: DMD frequency spectrum

the structures decreases. Thus, the high-end of the spectrum is less interesting as it is more representative of the smallest turbulent structures. Although $St \sim 0.3$ represents the lowest frequency resolvable with the chosen window size, it is nonetheless examined further. Future work should consider longer window lengths to increasing the low frequency resolution of the analysis.

The lowest frequency mode in the density field is shown in figure 3.9. As expected, the low-frequency is associated with the shock motion. In particular, this mode captures the dynamics of both the upstream separation and reattachment shock. The strong opposite magnitudes suggest that the motions of the two shocks are out of phase with one another. The mode shape and phase differences between the shocks agree well with the first density POD mode in figure 3.5. As mentioned before, Strouhal numbers associated with SWTBLI are usually in the region of 0.03 to 0.5. The frequency of this mode ($St_L \sim 0.3$) fits into

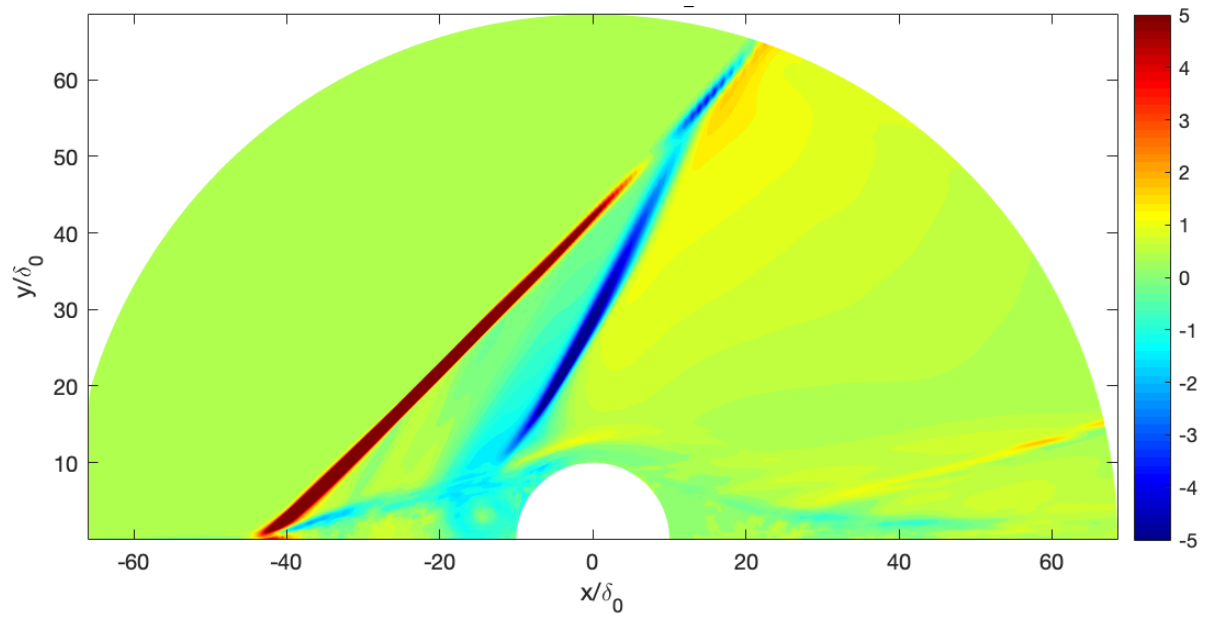

Figure 3.9: Density field low-frequency DMD Mode $St_L \sim 0.3$

this region, but is on the high end. It is expected that it would not cleanly fall into this category, as this DMD mode is capturing the motion of the two resulting shock waves, as opposed to just the interaction of one shock and the boundary layer. Furthermore, the length scales employed to obtain the Strouhal numbers are not the same. However, this mode was consistently non-trivial from window to window, which follows the same trend as SWTBLI spectral analysis.

The DMD mode at this same low-frequency ($St_L \sim 0.3$) was identified in the velocity decomposition and is shown in figure 3.10. Similar to the density mode, the two shock structures are easily identifiable; however, large oscillations in the separation regions and shear layers in front and behind the turret structure are now amplified. This suggests that these amplified regions have motion at the same low-frequency as shock waves and could be interacting with their unsteadiness. This shape is generally similar to what was identified in the first velocity POD mode seen in figure 3.6. The fact that the DMD and POD analyses extracted the same distinct shape indicates the dominance of this mode.

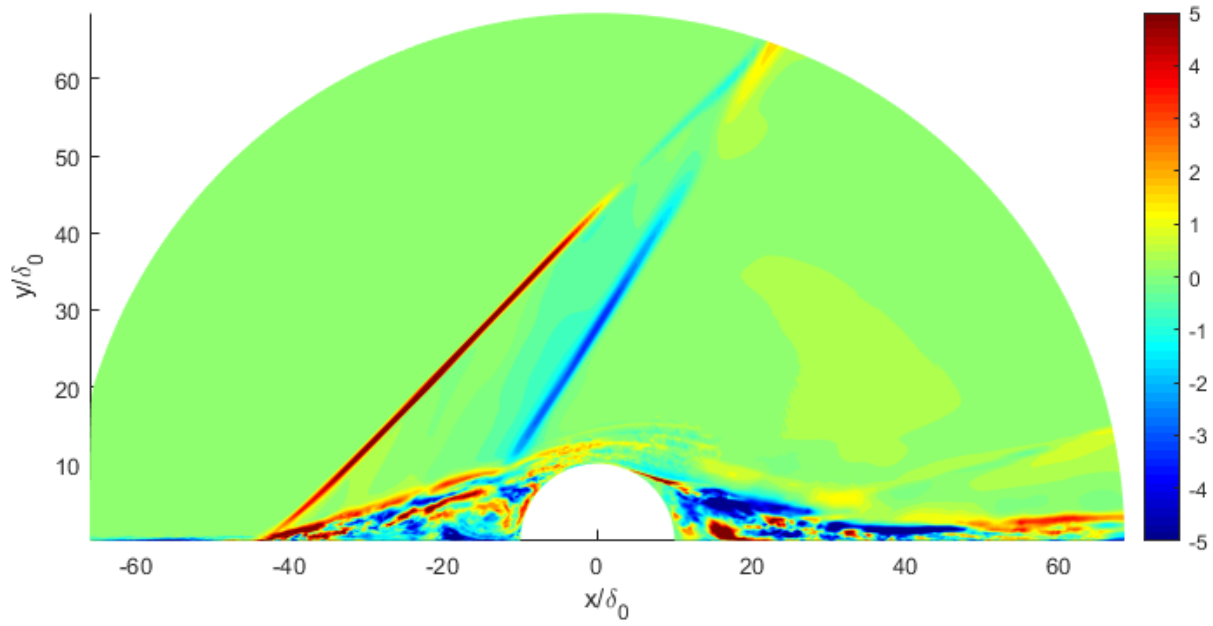

Figure 3.10: Streamwise Velocity field low-frequency DMD Mode $St_L \sim 0.3$

As mentioned, it is also important to identify structures besides the shocks that are still contributing to large fluctuations in the flow. Modes with intermediate frequencies and large amplitudes were also investigated. A coherent structure that dominated the intermediate frequency range in the density field is shown in figure 3.11. This mode reveals coherent shedding structures along the shear layer. Comparing this DMD mode to the higher order POD modes in figure 3.7, the structures along the shear layer are very similar. However, DMD extracts a more coherent, organized pattern since it highlights fluctuating structures associated at one frequency.

This same coherent oscillating pattern stays very prevalent through higher frequency modes; however, the structures decrease in size. This can be seen in the DMD mode in figure 3.12. A close examination of the mode indicates that the structures originate at the beginning of the incoming turbulent boundary layer. This mode has a frequency which is two orders of magnitude larger than the one associated with the shock motion, which is a common finding in SWTBLI simulations and experiments [25].

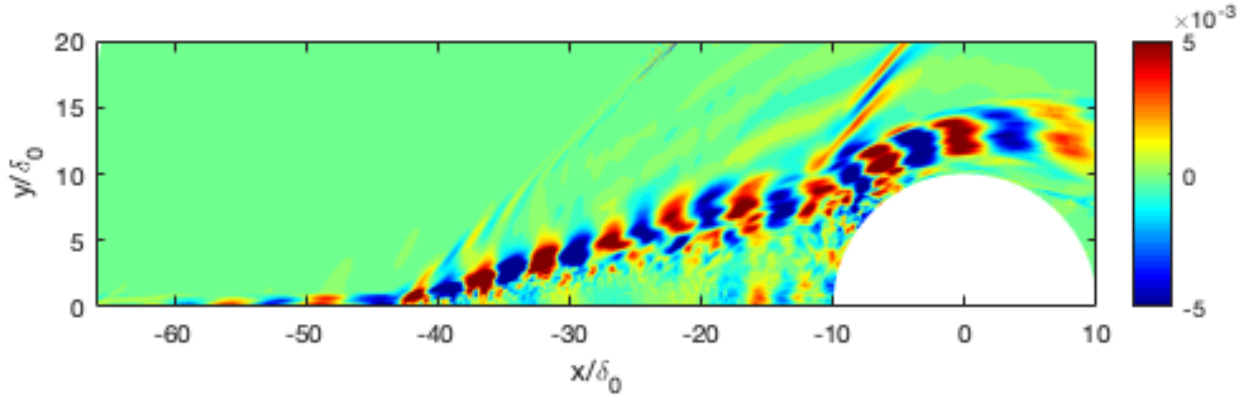

Figure 3.11: Density field intermediate-frequency DMD Mode $St_L \sim 11.5$

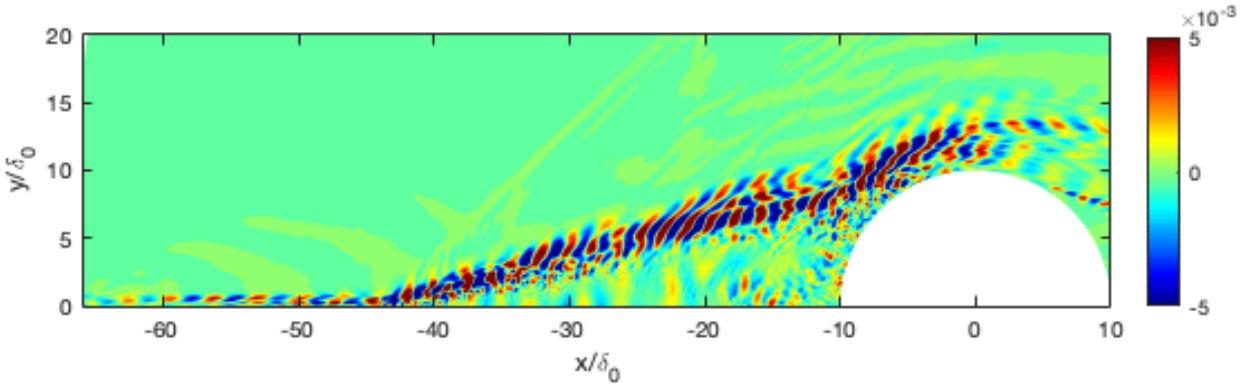

Figure 3.12: Density field high-frequency DMD Mode $St_L \sim 30$

Although the structures seen in figures 3.11 and 3.12 are much smaller in size than the shocks, the fact that this oscillating pattern continues through a range of frequencies is significant. The shear layer is turbulent and thus the shedding is broadband and multiscale. DMD shows that there is a coherent pattern across that range. This gives evidence that although the POD mode contributes relatively less to the features in this region, it was likely distributing it over many modes. Thus, the combination of POD and DMD analyses provides a good way to examine broadband as well as coherent patterns.

Chapter 4: Conclusion

Modal decomposition was used to analyze data from a large eddy simulation of supersonic flow over a wall mounted turret. Two methods were employed, the Proper Orthogonal Decomposition (POD) and the Dynamic Mode Decomposition (DMD). The goal was to investigate how modal decomposition could be used to study a fluid flow problem that contained a variety of unsteady features. In addition, the goal was to provide physical insight into a representative turbulent turret flow as a preliminary towards understanding flow control.

The POD analysis objectively ranked flow features based on their contribution to unsteadiness or 'energy' content. The top POD mode contained the motion of the two upstream unsteady shock waves and captured over 40% of the density variation in the flow. Similar shock shapes were found in the top modes of the velocity field, but with higher magnitudes also in the separated regions. This suggested that the oscillations in the separation regions could be contributing to the shock unsteadiness. Overall, the POD analysis gave evidence that the shock motion was dominating the unsteadiness in the flow.

The DMD analysis extracted modes that approximated how features in the flow were evolving, with each mode separated by a characteristic frequency. The unsteady shock motion was captured in the lowest-frequency mode, for both the density and velocity fields, at a non-dimensional frequency of $St_L = 0.3$. This low frequency motion agreed well with the trends normally seen in shock wave/turbulent boundary layer interactions. T he analysis also revealed intermediate frequencies that captured large fluctuations in the

The POD and DMD analysis both extracted modes the contained the motion of the separation and reattachment shock waves. The shapes captured in both methods agreed well with

one another and both revealed the two shocks moving out of phase. While the POD analysis was able to objectively identify that shocks were the most dominant unsteady feature, it was not able to provide information regarding dynamics. The DMD analysis was able to complement the POD analysis by providing detail about the dynamics of the shock motion, revealing a low-frequency that could be targeted for future flow control techniques.

The application of both the POD and DMD to the turret flow demonstrated how the methods complement each other. POD provides an understanding of the energy dominant modes, while DMD provides details about the dynamics of the flow structures. Although the flow application contained a variety of unsteady, multiscale features evolving at different frequencies, modal decomposition was able to characterize the dominant physics.

Appendix A: POD Matlab Code

```
%% read in data
load('Velocity_2000Snaps.mat')
data = u;
%% how many snapshots you want to decompose
nomv        = length(u(1,:));
% set i and j dimension
imax        = length(x(:,1));
jmax        = length(y(1,:));

%% PERFORM POD
%create snapshot matrix
clear s
s = data(:,1:nomv); % reshape data into a matrix with nomv rows
mean_flow = mean(s,1);
p = s - mean_flow;   % substract the mean from each row

% covariance matrix
C_s = (p'*p)/(nomv-1);

% Solve eigenvalue problem
[A_s, LAM_s] = eig(C_s,'vector');

% Sort eigenvalues and eigenvectors
[lambda_s,ilam_s] = sort(LAM_s,'descend');
```

```
25 A_s = A_s(:, ilam_s); % These are the temporal modes
26
27 % Calculate spatial coefficients
28 PHI_s = p*A_s;
29
30 % Normalization to match direct and snapshot modes (optional)
31 PHI = normc(PHI_s); % Spatial modes
32 A = p'*PHI;          % Time coefficients
33
34 % Calculate energy per mode
35 energy = lambda_s ./ sum(lambda_s);
36 total_energy = cumsum(energy);
37
38 %% Plot spatial modes
39 mode = 1;
40 % reshape recontruction
41 POD_Mode = reshape(PHI(:,mode),[imax jmax]);
42
43 % plot POD mode
44 figure()
45 contourf(x,y,POD_Mode,200,'linestyle','none')
46 t = [variable ': POD Mode ' num2str(mode)];
47 title(t)
48 colorbar
49 colormap jet
50 axis equal
```

Appendix B: DMD Matlab Code

```
%% Load Data
load('Velocity_2000Snaps.mat')
variable = 'Velocity';
%% Set i and j dimensions
imax = length(x(:,1));
jmax = length(y(1,:));

%% Create Snapshot Matrix - Big_X
Big_X = data;
numSnaps = length(Big_X(1,:)); % Number of snapshots
dims  = size(Big_X);

% Split Big_X into two snapshot sets
X1 = Big_X(:,1:end-1);
X2 = Big_X(:,2:end);

%% Perform DMD
% SVD on X - economy
[U, S, V]=svd(X1,'econ');

% Build reduced A matrix
Atilde      = U' * X2 * V / S; % low-rank dynamics

% Solve for DMD modes
```

```
25 [W_r, D]      = eig(Atilde);
26 Phi           = X2 * V / S * W_r; % modes
27
28 % solve for eigenvalues and frequencies/growth-rates
29 dt = .1;                        % time step in between snapshots
30 lambda  = diag(D);              % discrete-time eigenvalues
31 omega   = log(lambda)/dt;       % continous-time eigenvalues
32
33 % Compute DMD mode amplitudes
34 b = Phi\Big_X(:,1);
35
36 % Sort modes based on absolute scale
37 abs_b =abs(b)/max(abs(b));
38 [abs_scl_sort, SortIndex] = sort(abs_b,'descend');
39 % Sort modes, frequencies, growth rates according to mode
      amplitude
40 omega = omega(SortIndex);
41 growth_rate = real(omega);
42 freq = abs(imag(omega));
43 b = b(SortIndex);
44 for ip=1:1:length(b)
45     dmdmodes_sort(:,ip)=Phi(:,SortIndex(ip));
46 end
47
48 %% Plot magnitudes and frequency spectrum
49 modeNumbers = 1:length(b);
50 figure()
```

```
51 stem3(freq(3:end),modeNumbers(3:end),abs(b(3:end)))
52 zlabel('Magnitude')
53 xlabel('Frequency')
54 xlim([0  2])
55 t = [variable ' DMD Mode Magnitude and Frequencies'];
56 title(t)
57 view(0,0)
58
59 %% plot dmd mode of interest
60 a_mode = 1;
61 dmd_mode = reshape(dmdmodes_sort_mag(:,a_mode), [imax jmax]);
62
63 figure()
64 hold on
65 contourf(x,y,real(dmd_mode),100,'linestyle','none')
66 colorbar
67 colormap jet
68 axis equal
```

Bibliography

[1] Sadatoshi Taneda. "Experimental Investigation of the Wakes behind Cylinders and Plates at Low Reynolds Numbers". In: *Journal of the Physical Society of Japan* 11.3 (1956), pp. 302–307. DOI: 10.1143/JPSJ.11.302.

[2] B. W. van Oudheusden et al. "Phase-resolved characterization of vortex shedding in the near wake of a square-section cylinder at incidence". In: *Experiments in Fluids* 39.1 (July 2005), pp. 86–98. ISSN: 1432-1114. DOI: 10.1007/s00348-005-0985-5.

[3] Kunihiko. Taira. "Modal Analysis of Fluid Flows: An Overview". In: *AIAA* 55.12 (2017).

[4] Peter Schmid. "Application of the dynamic mode decomposition to experimental data". In: *Experiments in Fluids* 50 (Apr. 2011), pp. 1123–1130. DOI: 10.1007/s00348-010-0911-3.

[5] Tim Horchler, Karthik V. Mani, and Klaus Hannemann. "Dynamic Mode Decomposition of Backward Facing Step Flow Simulation Data". In: June 2015. DOI: 10.2514/6.2015-3411.

[6] Kunihiko Taira et al. *Modal Analysis of Fluid Flows: Applications and Outlook*. In: (2019). arXiv: 1903.05750 [physics.flu-dyn].

[7] J. N. Kutz et al. "Chapter 1: Dynamic Mode Decomposition: An Introduction". In: SIAM, 2016, pp. 1–24. DOI: 10.1137/1.9781611974508.ch1.

[8] Stefan Volkwein. "Proper Orthogonal Decomposition: Theory and Reduced-Order Modelling". In: *Lecture Notes, University of Konstanz* (Jan. 2012).

[9] Tomas W. Muld, Gunilla Efraimsson, and Dan S. Henningson. "Flow structures around a high-speed train extracted using Proper Orthogonal Decomposition and Dynamic

Mode Decomposition". In: *Computers and Fluids* 57 (2012), pp. 87–97. ISSN: 0045-7930. DOI: https://doi.org/10.1016/j.compfluid.2011.12.012.

[10] Vladimir Statnikov et al. "Analysis of pressure perturbation sources on a generic space launcher after- body in supersonic flow using zonal turbulence modeling and dynamic mode decomposition". In: *Physics of Fluids* 27 (Jan. 2015). DOI: 10.1063/1.4906219.

[11] Kunihiko Taira and Tim Colonius. "Three-dimensional flows around low-aspect-ratio flat-plate wings at low Reynolds numbers". In: *Journal of Fluid Mechanics* 623 (2009), pp. 187–207. DOI: 10.1017/S0022112008005314.

[12] J. L. Lumley. "The structure of inhomogeneous turbulence". In: *Turbulence and Wave Propagation* (1967), pp. 166–78.

[13] J. L. Lumley. G. Berkooz P. Holmes. "The proper orthogonal decomposition in the analysis of turbulent flows". In: *Annual Review of Fluid Mechanics* 25 (1993), pp. 539–575.

[14] Gaëtan Kerschen et al. "The Method of Proper Orthogonal Decomposition for Dynamical Characterization and Order Reduction of Mechanical Systems: An Overview". In: *Nonlinear Dynamics* 41 (Aug. 2005), pp. 147–169. DOI: 10.1007/s11071-005-2803-2.

[15] Moritz Sieber, C. Oliver Paschereit, and Kilian Oberleithner. "Spectral proper orthogonal decomposition". In: *Journal of Fluid Mechanics* 792 (2016), pp. 798–828. DOI: 10.1017/jfm.2016.103.

[16] C. W. Rowley. "Model Reduction For Fluids, Using Balanced Proper Orthogonal Decomposition". In: *International Journal of Bifurcation and Chaos* 15.03 (2005), pp. 997–1013. DOI: 10.1142/S0218127405012429.

[17] P.J Schmidt. "Dynamic mode decomposition of numerical and experimental data". In: *Journal of Fluid Mechanics* 656 (2010), pp. 5–28.

[18] Clarence W. Rowley et al. "Spectral analysis of nonlinear flows". In: *Journal of Fluid Mechanics* 641 (2009), pp. 115–127. DOI: 10.1017/S0022112009992059.

[19] M.R. Jovanovic, P.J. Schmid, and J.W. Nichols. "Sparsity-promoting dynamic mode decomposition". In: *Physics of Fluids* 26 (2 2014).

[20] Philip E. Morgan and Miguel R. Visbal. "Numerical Simulation Exploring Supersonic Flow Over a Forward-Facing Cylindrical Step". In: *45th AIAA Fluid Dynamics Conference*. 2015. DOI: 10.2514/6.2015-2640.

[21] Philip Morgan, Scott Sherer, and Miguel Visbal. "Numerical Investigation of Supersonic Flow Over a Wall-Mounted Cylinder". In: Jan. 2016. DOI: 10.2514/6.2016-0046.

[22] Philip E. Morgan, Scott E. Sherer, and Miguel Visbal. "Numerical Exploration of Supersonic Flow Over a Wall-Mounted Hemisphere". In: *46th AIAA Fluid Dynamics Conference*. 2016. DOI: 10.2514/6.2016-3650.

[23] Philip E. Morgan, Scott E. Sherer, and Miguel R. Visbal. "Parametric study of supersonic flow over a wall-mounted hemisphere". In: *2018 AIAA Aerospace Sciences Meeting*. 2018. DOI: 10.2514/6.2018-1786.

[24] Stanislav Gordeyev and Eric Jumper. "Fluid dynamics and aero-optics of turrets". In: *Progress in Aerospace Sciences* 46.8 (2010), pp. 388–400. ISSN: 0376-0421. DOI: https://doi.org/10.1016/j.paerosci.2010.06.001.

[25] Noel T. Clemens and Venkateswaran Narayanaswamy. "Low-Frequency Unsteadiness of Shock Wave/Turbulent Boundary Layer Interactions". In: *Annual Review of Fluid Mechanics* 46.1 (2014), pp. 469–492. DOI: 10.1146/annurev-fluid-010313-141346.

[26] Lawrence Sirovich. "Turbulence and the dynamics of coherent structures. I - Coherent structures". In: *Quarterly of Applied Mathematics* 45 (1987). DOI: 10.1090/qam/910463.

[27] Roger A. Horn and Charles R. Johnson. *Matrix Analysis*. Cambridge University Press, 1990. ISBN: 0521386322.

[28] Jonathan H. Tu et al. “On dynamic mode decomposition: Theory and applications”. In: *Journal of Computational Dynamics* 1.2 (Dec. 2014), pp. 391–421. ISSN: 2158-2491. DOI: 10.3934/jcd.2014.1.391.